Iranian Journal of Chemistry and Chemical Engineering (IJCCE)

In situ preparation of CeO_2/Bi_2WO_6 nanocomposite and its brilliant catalytic activity for reduction of dye pollutants, Chromium (VI), 4-nitrophenol and 4-nitroaniline

Ahmad Amani [a], Zohreh Derikvand,*[,b], Mohammad Ghadermazi**[,a]

[a] *Department of Chemistry, Faculty of Science, University of Kurdistan, Sanandaj, Iran*

[b]*Department of Chemistry, Khorramabad Branch, Islamic Azad University, Khorramabad, Iran*

*e-mail: zderik@yahoo.com

**e-mail: mghadermazi@yahoo.com

IJCCE-Accepted Article

ABSTRACT*: The CeO_2/Bi_2WO_6 nanocomposite was synthesized using sonochemical and hydrothermal methods. It was studied for its catalytic activity in reducing 4-nitrophenol (4-NP), 4-nitroaniline (4-NA), chromium (VI), rhodamine B(RhB) and methylene blue (MB) in aqueous solutions. Analytical techniques like Fourier transform infrared (FT-IR) spectroscopy, photoluminescence (PL) spectroscopy, Brunauer-Emmett-Teller (BET), X-ray diffraction (XRD), transmission electron microscopy (TEM), UV–visible diffuse reflectance spectroscopy (DRS), energy dispersive X-ray spectroscopy (EDX) and scanning electron microscopy (SEM) were used to characterize the nanocomposites. The CeO_2/Bi_2WO_6 10% composite showed the most effective results, achieving complete reduction of 4-nitrophenol in 10 minutes. The nanocomposite also demonstrated impressive recyclability, indicating its potential for practical applications.*

Keywords: *4-Nitroaniline, 4-Nitrophenol, Chromium(VI), CeO_2, Rhodamine B, Mehthylen blue*

INTRODUCTION

Metal tungstates and their nanocomposites have earned significant attention in various fields, such as optical devices, optoelectronics, photoluminescence, catalysis, and sensing owing to their unique structure and exceptional physical and chemical properties [1-6]. Among these materials, bismuth tungstate (Bi_2WO_6) stands out as a significant n-type semiconductor with a narrow band gap, offering promising prospects, including excellent photocatalytic activity, ferroelectricity, piezoelectricity, and nonlinear dielectric susceptibility [7-9]. Various synthesis methods, such as template-assisted, sol-gel, hydrothermal, solvothermal, sonochemical and co-precipitation, produced Bi_2WO_6 nanostructures with diverse morphologies [10-14]. Organic pollutants from industries like food, textile, and leather pose a significant environmental threat, and nanocomposites have emerged as effective solutions for their degradation. Bi_2WO_6 and its nanocomposites are being investigated for their potential to degrade dyes and other pollutants [8, 12].

4-Nitrophenol (4-NP) and its derivatives are crucial in synthetic dyes, pesticides, and herbicides production, but their widespread use poses a significant environmental and human health threat [15-19]. This contamination can lead to severe consequences for both ecosystems and human well-being, including eye irritation, loss of consciousness, and potential carcinogenic effects [20]. Therefore, the urgent need to remove 4-NP from the environment is undeniable. Various technologies have been employed to address this challenge, including thermal degradation, adsorption, electrocoagulation, photodegradation, ozonation, electrochemical degradation, and the electro-Fenton method, as well as biodegradation [21-26]. These approaches often suffer from drawbacks such as prolonged treatment times, generation of secondary pollutants, high costs, low efficiency, and adverse environmental impacts [27-30], prompting the exploration of alternative methods [31]. Among these alternatives, catalytic reduction using $NaBH_4$ stands out as a particularly promising and environmentally friendly approach to converting nitrophenol to aminophenol [32-34]. This reduction reaction has garnered significant attention due to the production of 4-aminophenol, an intermediate with diverse industrial applications in medicine, rubber manufacturing, dye production, photography, and anti-corrosion lubricants [34-38].The conversion of 4-NP to amine offers significant advantages in industrial, environmental, and economic aspects, necessitating the development of efficient catalysts with robust adsorption capacity and affordability. Textile industry dyes pose a significant global water pollution threat due to their toxic, nondegradable nature, posing a significant threat to human health and the environment [39, 40].

Chromium (VI) ions represent a severe contaminant in industrial wastewater originating from various processes for example paint manufacturing, electroplating, and leather tanning. Due to their high mobility in water and their profoundly toxic, mutagenic, and carcinogenic properties, the imperative task at hand is their removal from wastewater sources [41, 42]. Typically, the treatment of chromium (VI) involves a reduction step to chromium (III), which is substantially less toxic and even serves as a vital trace metal in human nutrition [43-45].

Recent focus has centred on metal oxide nanoparticles due to their remarkable catalytic performance [34, 43-45], by loading nanoparticles onto substrates, specific physical and chemical properties are enhanced, boosting their catalytic activity [34, 46, 47]. The study incorporated CeO_2 (5, 10, and 20 weight %) into Bi_2WO_6 structure to improve catalytic activity. The resulting CeO_2/Bi_2WO_6 nanocomposite effectively reduced dye pollutants (RhB and MB), 4-nitrophenol, 4-nitroaniline, and Cr(VI) ions using $NaBH_4$. The nanocomposites' catalytic activity is influenced by CeO_2 concentration, offering recyclability, reusability, simplicity, stability, strong catalytic activity, and green chemistry adherence.

IJCCE-Accepted Article

EXPERIMENTAL SECTION

Chemical reagents

Bismuth nitrate, Cerium (III) nitrate hexahydrate, Nitric acid (HNO_3 37%), cethyltrimethylammonium bromide (CTAB) ($C_{19}H_{42}BrN$), potassium dichromate ($K_2Cr_2O_7$), Ethanol, Sodium hydroxide (NaOH), 4-Nitrophenol (4-NP) ($C_6H_5NO_3$), 4-Nitroaniline (4-NA) ($C_6H_6N_2O_2$), $NaBH_4$, methylene blue (MB), rhodamine B (RhB), Sodium tungstate (Na_2WO_4) were used as received (Merck company (Germany)).

Preparation of Bi_2WO_6

To prepare Bi_2WO_6, 8 ml of 0.1 M HNO_3 was added to an aqueous solution of bismuth nitrate (0.03g in 20 ml distilled water) and stirred till a clear solution was obtained. After that, (0.24 g) of cethyltrimethylammonium bromide (CTAB) under vigorous stirring was added to the above solution. Then, an aqueous solution of sodium tungstate (0.1 g in 10 ml distilled water) with 0.24 g CTAB was prepared under stirring for 10 minutes. The bismuth nitrate solution was added dropwise to the sodium tungstate solution. The pH of solution was carefully adjusted to 7 using a NaOH (1M) solution. The resulting white emulsion was moved to a 50 ml autoclave and kept at 180°C for 24 hours. The prepared precipitate was filtered, thoroughly washed several times with water/ethanol, and put in an oven at 80 °C for 8 hours.

Preparation of CeO_2/Bi_2WO_6 nanocomposites

To synthesize the CeO_2/Bi_2WO_6 nanocomposites, a well-defined procedure was followed. Initially, 8 mL of 0.1 M HNO_3 was added into an aqueous solution containing bismuth nitrate (0.22g) and the mixture was stirred until a clear solution was achieved. Subsequently, 0.24 g of cetyltrimethylammonium bromide (CTAB) was added under vigorous stirring, for 30 minutes. In parallel, an aqueous solution of sodium tungstate (0.1 g in 10 ml distilled water) was prepared, incorporating 0.24 g of CTAB, and stirred for 30 minutes. The bismuth nitrate solution was then added dropwise to the sodium tungstate solution with continuous magnetic stirring. The pH of solution was carefully adjusted to 7 using a NaOH (1M) solution. Different weight percentages of CeO_2 (5, 10 and 20 weight %) were combined to the resulting white gel of Bi_2WO_6 under ultrasonically treated for 2 hours. Then, the resulting gel was transferred to the autoclave with 50 ml capacity and kept at 180°C for one day. After being naturally cooled, the solid powder was collected and washed with DI-H_2O and EtOH and put at 80°C for 8 hours. The white color of the Bi_2WO_6 turned yellow.

Instrumentation

The FT-IR spectra were *obtained* using a Perkin-Elmer Spectrum RXI FT-IR spectrophotometer. XRD analyses were conducted using X-ray diffractometer (PANalytical/X'Pert Pro MPD) with a wavelength (λ) of 1.5406 Å. UV-vis spectra were acquired through a Perkin-Elmer Lambda 25 UV-vis spectrophotometer. To explore the morphology and size of the CeO_2/Bi_2WO_6 nanocomposites, an in-depth examination was performed using a MIRA3 TESCAN field emission scanning electron microscope (FESEM) equipped with an associated energy dispersive X-ray (EDX) analyzer. The surface area of the synthesized nanocomposite was evaluated by BET model. Additionally, BJH method was employed to investigate the pore size and volume pore distribution of the

IJCE-Accepted Article

nanocomposite. The photoluminescence (PL) properties of the samples were analyzed by a Varian Cary Eclipse fluorescence spectrometer at room temperature. TEM was investigated by an EM10C–100 kV series microscope.

Catalytic activities test for reducing 4-nitrophenol and 4-nitroaniline

The catalytic efficacy of the CeO_2/Bi_2WO_6 nanocomposites in reducing 4-nitrophenol and 4-nitroaniline with an excess of $NaBH_4$ was systematically explored in a quartz cell at ambient temperature. The catalytic reduction of 4-nitrophenol (4-NP) utilizing $NaBH_4$ served as a model reaction, and the reaction progress was monitored by UV-vis spectroscopy. For the catalytic assessment, a quartz cell containing 2 mL of 4-NP (0.2 mM) was utilized. Then, 0.5 mL of $NaBH_4$ (20 mM) and 1 mg of the CeO_2/Bi_2WO_6 nanocomposite was added into the reaction mixture. Subsequently, at 2-minute intervals, the conversion of 4-NP was investigated within the scanning range of 200-500 nm. Upon completion of the reaction, the catalyst was separated from the solution, subjected to multiple washes with deionized water (DI-H_2O), and then dried for subsequent cycles. Equations (1) and (2) were employed to calculate the rate constant and conversion efficiency.

$$K_t = - \ln \frac{C_t}{C_0} \quad (1)$$

$$R(\%) = \frac{C_0 - C_t}{C_0} \times 100 \quad (2)$$

Investigation of Cr(VI) catalytic reduction

A stock solution of Cr(VI) at a concentration of 0.1 mM was prepared by dissolving $K_2Cr_2O_7$ in deionized H_2O. Subsequently, 2 mL of this solution was transferred into a quartz cell, and its absorption spectra were recorded using a UV-visible spectrophotometer in the range of 200-600 nm. The Cr(VI) ions in the aqueous solution exhibited a distinctive absorption peak at 373 nm. To observe the changes in the absorption peak at 373 nm, 0.5 mL of $NaBH_4$ (20 mM) and 1 mg of the CeO_2/Bi_2WO_6 nanocomposite was introduced into the quartz cell and the UV-visible spectrum was monitored at 2-minute intervals. The influence of only the reducing agent ($NaBH_4$) and only the CeO_2/Bi_2WO_6 nanocomposite on reducing Cr(VI) ions was systematically investigated.

Catalytic reduction of dyes

The methylene blue and rhodamine B dye stock (0.2 mM) solution were prepared by dissolving a proper amount of dyes (0.2 mM) in deionized water. The progress of dyes reduction by CeO_2/Bi_2WO_6 nanocomposite in the present and absence of $NaBH_4$ was monitored via UV-vis.

RESULTS AND DISCUSSION

Optimization of the synthesis conditions

This study investigated the impact of various operational variables, for instance temperature, pH, and reaction duration, on the fabrication of nanocomposites to determine the most favorable synthesis conditions. We investigated the pH values ranging from 5 to 9, with the most favourable outcome achieved at pH 7. The impact of varying reaction durations between 8 to 24 hours was studied at temperatures ranging from 90°C to 180°C. The results revealed that a pure CeO_2/Bi_2WO_6 nanocomposite was only achieved at 180°C after 24 hours. It was observed that lower temperatures led to the formation of a multi-phase structure instead. Furthermore, the

IJCE-Accepted Article

concentration of $NaBH_4$ in the catalytic experiments was analyzed, with the optimal concentration of 20 mM. Lower concentrations of $NaBH_4$ resulted in insufficient progress of the reduction reaction, while higher concentrations led to an immediate reaction that was difficult to monitor.

Characterization of CeO_2/Bi_2WO_6 nanocomposite

The FT-IR spectrum of CeO_2/Bi_2WO_6 was analyzed across the 400-4000 cm^{-1} range to determine the chemical bonds and functional groups present within the nanocomposite (Fig. 1a). A band at 722 cm^{-1} is indicative of the W-O stretching vibration within Bi_2WO_6. Additionally, characteristic peaks corresponding to Bi–O stretching and W–O–W bridging stretching are discernible at 561 cm^{-1} and 1361 cm^{-1}, respectively [48, 49, 4]. Notably, peaks associated with H-O-H bending and free OH stretching vibration emerge at 1610 cm^{-1} and 3416 cm^{-1}, respectively. These bands confirm the presence of water molecules physically adsorbed onto the surface of the nanocomposite. Furthermore, faint bands observed around 561 cm^{-1} and 433 cm^{-1} are attributable to Ce-O stretching vibration [50, 4].

The XRD pattern of the CeO_2, Bi_2WO_6 and CeO_2/Bi_2WO_6 nanocomposite are shown in Fig. 1b. Bi_2WO_6 has strong diffraction peaks at 2θ =28.50°, 32.92°, 47.26° and 58.65°, corresponding to (131), (200), (202) and (133) diffraction planes, respectively. All the diffraction peaks can be indexed to orthorhombic Bi_2WO_6 according to the JCPDS card no. 39-0256 [48]. In Fig. 1b, the XRD pattern of the nanocomposite reveals the presence of CeO_2 nanocubes. All diffraction peaks of CeO_2 are related to a FCC structure (JCPDS 89–8436). The characteristic peaks at 2θ angles of 28.50°, 47.26°, 58.65°, 68.82°, 76.22°, and 79.18° correspond to the reflection planes (111), (200), (220), (311), (222), (400), (331), and (420), respectively [51]. The sharp and intense diffraction peak indicates the sample's high crystallinity. As depicted in Fig. 1b, the CeO_2/Bi_2WO_6 nanocomposite exhibits the coexistence of Bi_2WO_6 and CeO_2 phases without any impurity phase [4, 5]. Figs. 2a and b show the results of FE-SEM analysis, revealing the surface morphology, size, and shape of the nanocomposite. The SEM images in Figs. 2a and b illustrate that the nanocomposite comprises nanorods decorated with cube nanoparticles. The average diameter of the nanorods is about 24.76 nm. Figs. 2c and d show TEM images of CeO_2/Bi_2WO_6 10% nanocomposite. It is evident from the images that particles exhibit nanorods morphology. To further investigate the elemental distribution and composition of the CeO_2/Bi_2WO_6 10% nanocomposite, EDX mapping measurements were conducted (Fig. 3).

IJCCE-Accepted Article

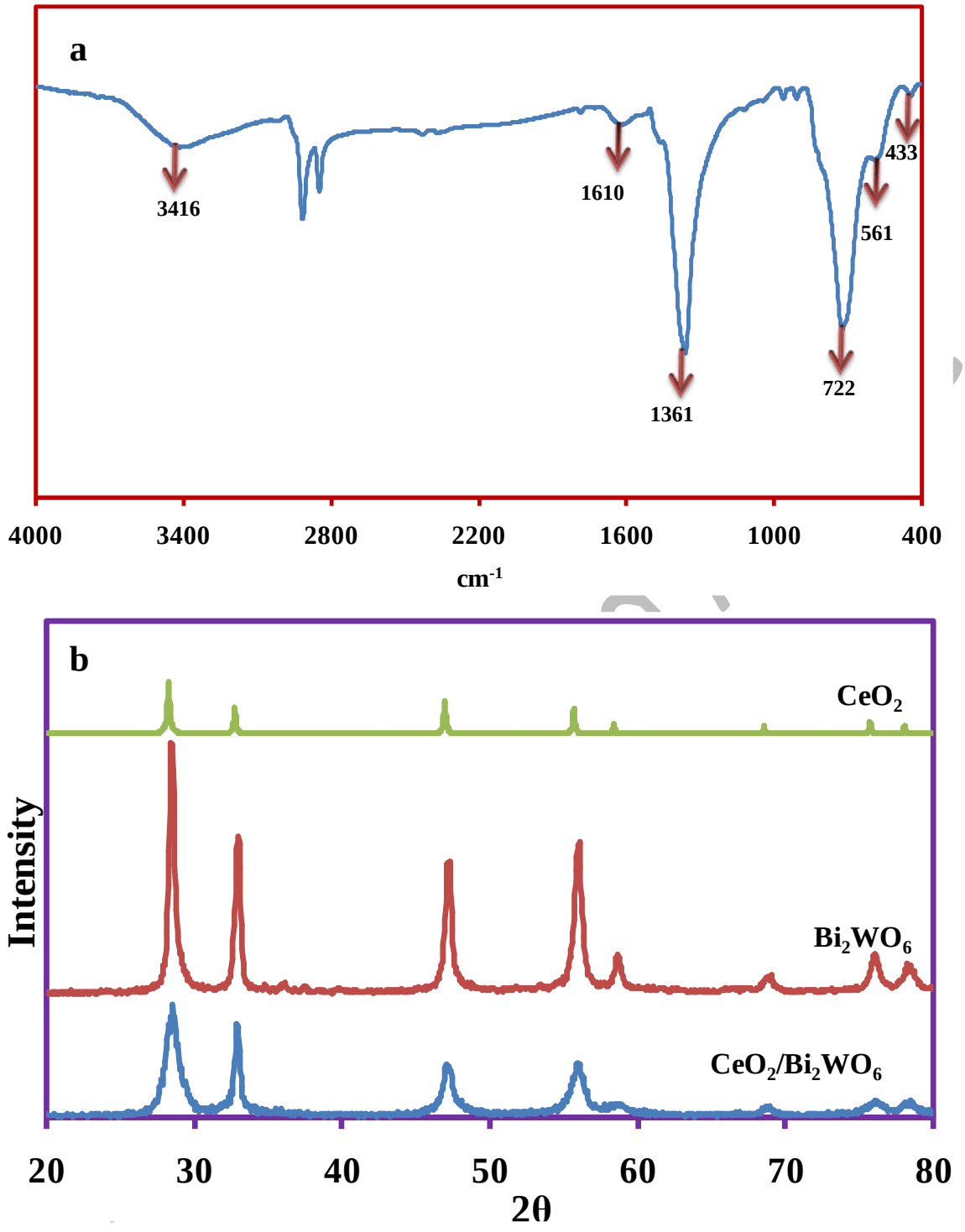

Fig. 1 (a) FT-IR spectra of CeO_2/Bi_2WO_6 nanocomposite, (b) XRD pattern of pure Bi_2WO_6, CeO_2 and CeO_2/Bi_2WO_6 nanocomposite.

The examination of surface texture and pore structure in the CeO_2/Bi_2WO_6 10% nanocomposite was conducted by analysing nitrogen adsorption-desorption isotherms. As illustrated in Fig. 4a, the nitrogen adsorption-desorption isotherms of the CeO_2/Bi_2WO_6 10% nanocomposite exhibit a type IV isotherm (hysteresis loop) with an H_3 hysteresis loop initiating at P/P0<0.4. This observation signifies the existence of a mesoporous structure. The characteristics of the nanocatalyst's surface texture and pore distribution significantly impact its catalytic

activities. The average pore diameter, total pore volume and specific surface area of the CeO_2/Bi_2WO_6 10% nanocomposite were measured at 27 nm, 0.174 cm^3/g and 25 m^2/g respectively. Estimating pore size distributions in the nanocomposite was accomplished using BJH method.

The UV-visible absorption spectra of CeO_2, Bi_2WO_6 and CeO_2/Bi_2WO_6 10% nanocomposite were analyzed to examine their optical properties (Fig. 4b). Pure CeO_2 and Bi_2WO_6 samples exhibited broad absorption peaks at 300 nm and 307 nm, respectively. The absorption characteristics of CeO_2 varied based on their morphologies and sizes [4, 5]. The UV absorption capacity of CeO_2 is linked to its band gap energy, which is crucial for understanding its optical properties. The UV-vis spectrum of the pure Bi_2WO_6 sample demonstrated high absorption in the UV-visible region, with an absorption edge at 307 nm owing to the intrinsic band-gap transition from the hybrid orbitals of O 2p and Bi 6s to the W 5d orbital. In contrast, the CeO_2/Bi_2WO_6 10% nanocomposite exhibited lower absorption in the UV-visible spectrum, with an absorption edge at 254 nm. The band gap energy was calculated by plotting the absorption coefficient $(\alpha hv)^n$ against photon energy (hv), where α is the absorption coefficient and E_g represents the band gap energy. The E_g values of CeO_2, Bi_2WO_6 and CeO_2/Bi_2WO_6 10% samples were 3.3, 3.2, and 2.9 eV, respectively, as shown in Fig. 4c through a Tauc plot. The Eg of Bi_2WO_6 decreased when loaded with CeO_2 nanoparticles, indicating that adding CeO_2 altered the band gap of Bi_2WO_6.

Fig. 4d shows PL spectra of CeO_2, Bi_2WO_6 and CeO_2/Bi_2WO_6 10% samples. In this study, the PL peak intensity of CeO_2/Bi_2WO_6 10% nanocomposite is lower than that of the as-prepared CeO_2 and Bi_2WO_6 samples. The PL spectrum of CeO_2 shows a prominent peak at 368 nm and one small peak at 577 nm. In cubic structure of CeO_2, the oxygen ions are not closely packed for which ceria form many oxygen vacancies. Ce^{3+} is present in the grain boundary. The presence of Ce^{3+} acts as a hole trap and oxygen vacancy as an electron trap. These two undergoes radiative recombination results in the 577 nm emission peak. . The PL intensity was observed to be more in pure sample compared to CeO_2/Bi_2WO_6 nanocomposite [4]. The results illustrated that the recombination rate of photoinduced charge carriers of CeO_2 /Bi_2WO_6 nanocomposites was less than that of pure CeO_2 and Bi_2WO_6 samples.

IJCCE-Accepted Article

a

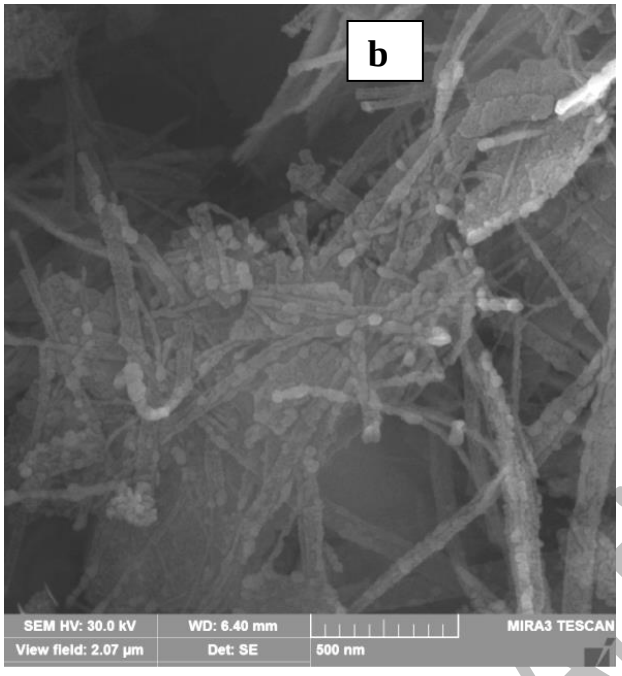

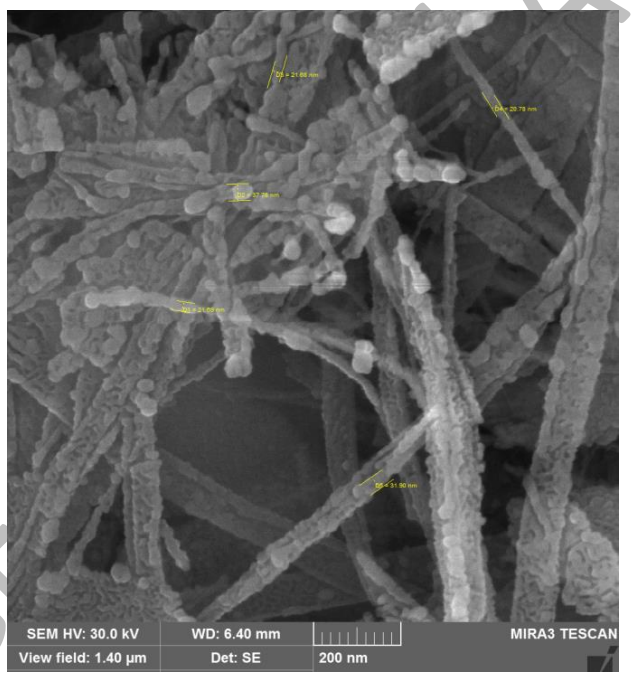

IJCE Article

Fig. 2 SEM (a, b) and TEM (c, d) images of CeO_2/Bi_2WO_6 nanocomposite.

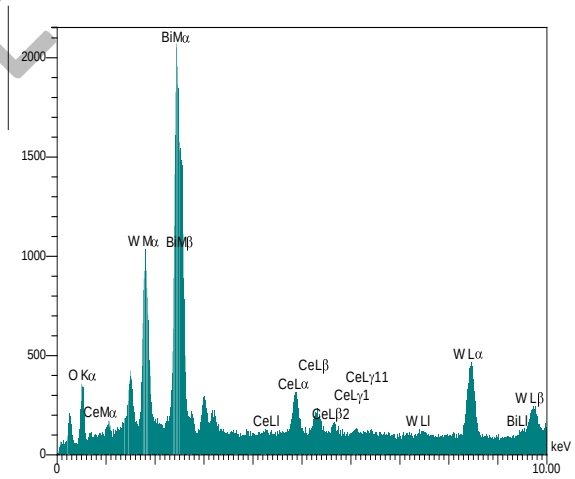

Fig. 3 EDX pattern of CeO_2/Bi_2WO_6 nanocomposite.

IJCCE-Article

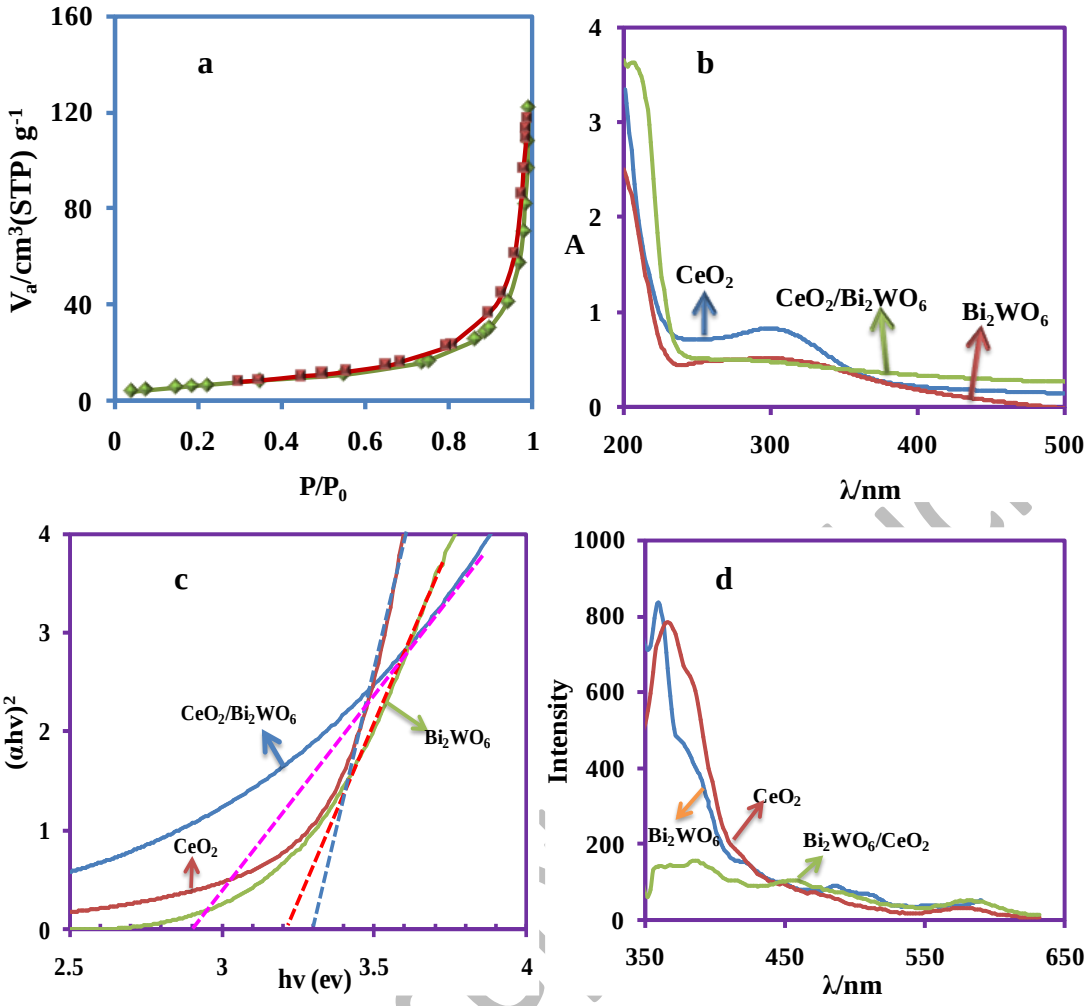

Fig. 4 (a) N_2 adsorption-desorption isotherm of CeO_2/Bi_2WO_6 10%nanocomposite, (b) UV-Vis of all samples and (c) Tauc plot of pure samples and CeO_2/Bi_2WO_6 10% nanocomposite, (d) PL spectra of CeO_2, Bi_2WO_6, and CeO_2/Bi_2WO_6 10% nanocomposite.

Catalytic reduction of nitroaromatic compounds

The synthesized CeO_2/Bi_2WO_6 nanocomposites catalyzed nitroaromatic compounds using $NaBH_4$ as the reductant. Typically, a UV–vis spectrum of a 4-nitrophenol solution displays a broad peak at 317 nm. This peak shifts to 400 nm when $NaBH_4$ was introduced to the reaction mixture, because of the formation of 4-nitrophenolate anions [32-34]. Interestingly, the peak intensity at 400 nm remains constant for up to 48 hours, indicating that the reduction of 4-nitrophenol has not occurred in the absence of a catalyst. This stagnation could be attributed to a high kinetic barrier between the donor and acceptor molecules (BH_4^- and 4-NP, respectively). Consequently, adding a catalyst to the reaction mixture becomes necessary to overcome this kinetic barrier, enabling the monitoring of the reduction reaction through UV–vis analysis. Therefore, similar experiments were conducted using the 4-NP-$NaBH_4$ solution. Upon introducing the nanocomposite into the reaction mixture, the peak intensity at 400 nm begins to decrease. Over time, a new peak appears at 300 nm in the UV–visible spectra (Fig.5). This shift is attributed to the formation of 4-aminophenol (4-AP) [32-34].

UCCE-Accepted

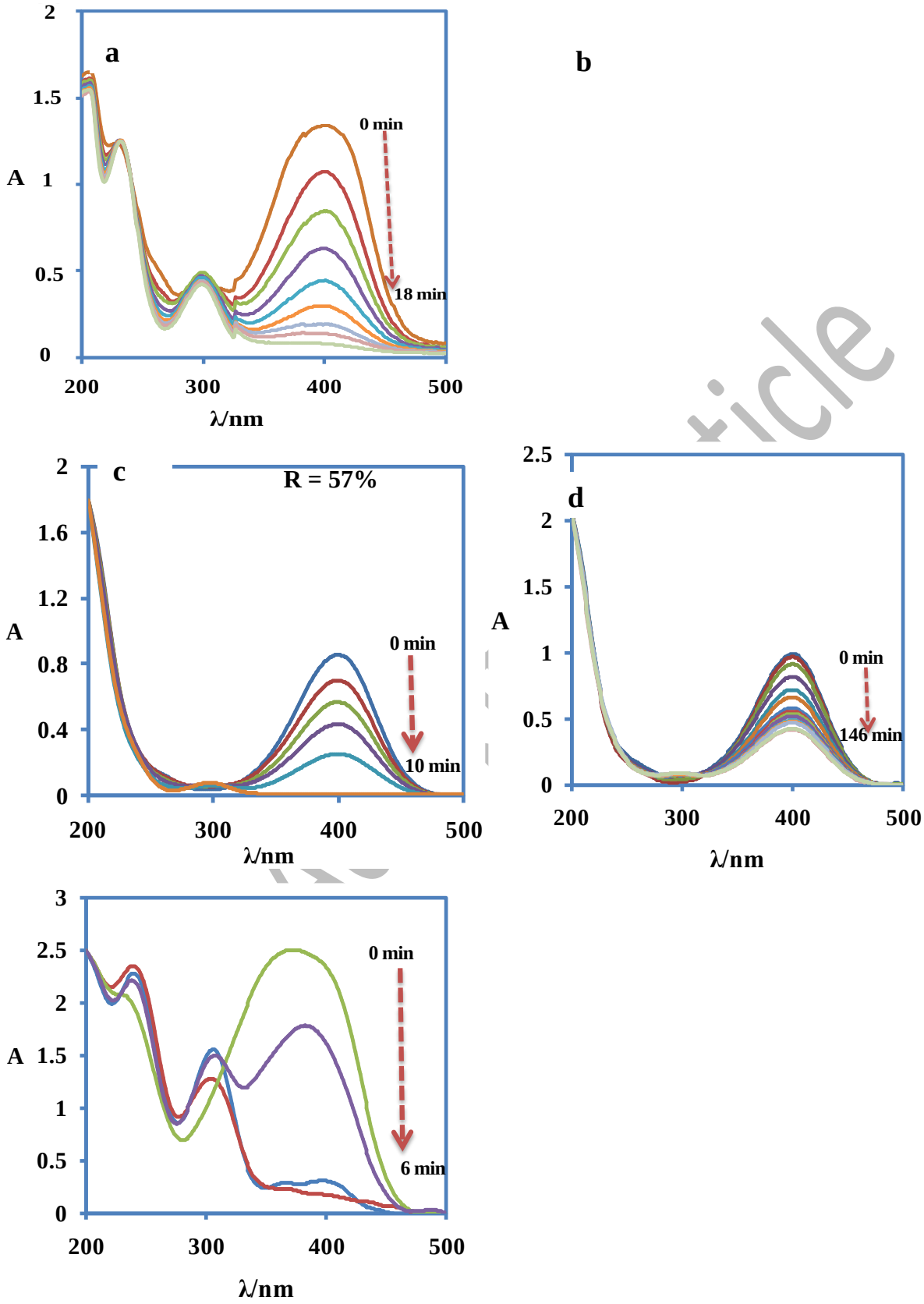
a
b
c
d
R = 57%
A
λ/nm
0 min
18 min
10 min
146 min
6 min

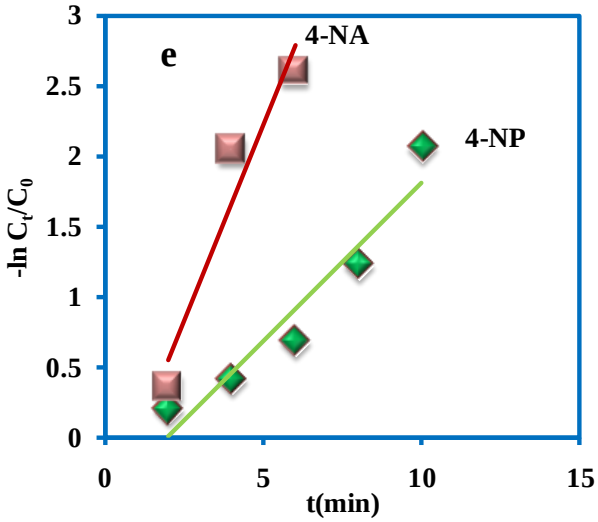

Fig.5 UV-vis spectral for reducing 4-NP (a) CeO_2/Bi_2WO_6 5%, (b) CeO_2/Bi_2WO_6 10%, (c) CeO_2/Bi_2WO_6 20% and (d) 4-NA with CeO_2/Bi_2WO_6 10% (with 0.5 mL $NaBH_4$ 20 mM and 1 mg CeO_2/Bi_2WO_6 nanocomposites), (c) plot showing pseudo-first-order kinetic for 4-NP and 4-NA with CeO_2/Bi_2WO_6 10 % .

The reduction reaction of 4-NP was completed within 18 minutes and 10 minutes in the presence of CeO_2/Bi_2WO_6 5 %, and CeO_2/Bi_2WO_6 10 % nanocomposites **,** respectively. The reduction reaction using the same amount of CeO_2/ Bi_2WO_6 20% nanocomposite was found to be prolonged, taking over 150 minutes to complete with a TOC of approximately 57% (Fig. 5c). The results show that the speed of the reduction reaction decreased when the CeO_2 dosage frequently increased from 10 % to 20 %. Most likely, the large quantity of CeO_2 assemble on the surfaces of Bi_2WO_6, which be able to coat Bi_2WO_6 active sites for 4-NP adsorption and fasten the synergetic effects between CeO_2 and Bi_2WO_6, as a result reduce the catalytic speed of the reduction reaction. The best catalytic efficiency of CeO_2/Bi_2WO_6 10% nanocomposite could be attributed to close contact between CeO_2 and Bi_2WO_6, which facilitates the electron transfer. The mixture of CeO_2 nanoparticles and Bi_2WO_6 in the solution offers more active sites for the formation of H_2 and e^- (from $NaBH_4$) on the surface of CeO_2/Bi_2WO_6 10 %, giving rise to increased reaction rate. Here 10 % weight of CeO_2 is considered as optimum loading on the surface of Bi_2WO_6. The findings indicate a notable acceleration in the reduction reaction rate with increasing amounts of CeO_2/Bi_2WO_6 10% nanocatalyst, completing the reaction in just 1 minute. Accordingly, we selected 1 mg of catalyst as the optimal quantity for subsequent experiments. The augmentation of CeO_2/Bi_2WO_6 10% nanocatalyst quantity facilitates greater accessibility to active sites for 4-NP adsorption, thereby enhancing the reduction reaction rate. The superior catalytic efficiency of the CeO_2/Bi_2WO_6 10% nanocomposite can be allocated to the intimate contact between CeO_2 and Bi_2WO_6, facilitating electron transfer from BH_4^- to 4-NP. The synergistic effect of Bi_2WO_6 and CeO_2 within the nanocomposite increases the availability of active sites for the formation of H_2 and e^- (from $NaBH_4$) on the surface of CeO_2/Bi_2WO_6 10%, consequently accelerating the reduction reaction rate. Primarily, H atoms/H_2 molecules are produced by reacting BH_4^- ions with water [33, 34]. These molecules and 4-nitrophenol are adsorbed simultaneously onto the surface of the $CeO_2/Bi_2WO_6$10% nanocomposite. The nano-sized particles within the CeO_2/Bi_2WO_6 10% nanocomposite facilitate electron transfer to 4-NP, effectively overcoming the reaction kinetic barrier. BH_4^- ions adsorb onto the nanocomposite surface, releasing hydrogen as hydride. The H^- anion then transfers to the metal particles within the nanocomposite, forming a complex.

IJCCE-Accepted Article

Concurrently, the nitro group of the 4-nitrophenolate ion is reduced by capturing the hydride from the complex. After three hydro-deoxygenation reactions, 4-AP is generated from 4-hydroxylaminophenol, a stable intermediate. In the final step, 4-AP is desorbed from the nanocomposite's surface, resulting in the ultimate reduction of 4-nitrophenol within the reaction mixture (Scheme 1).

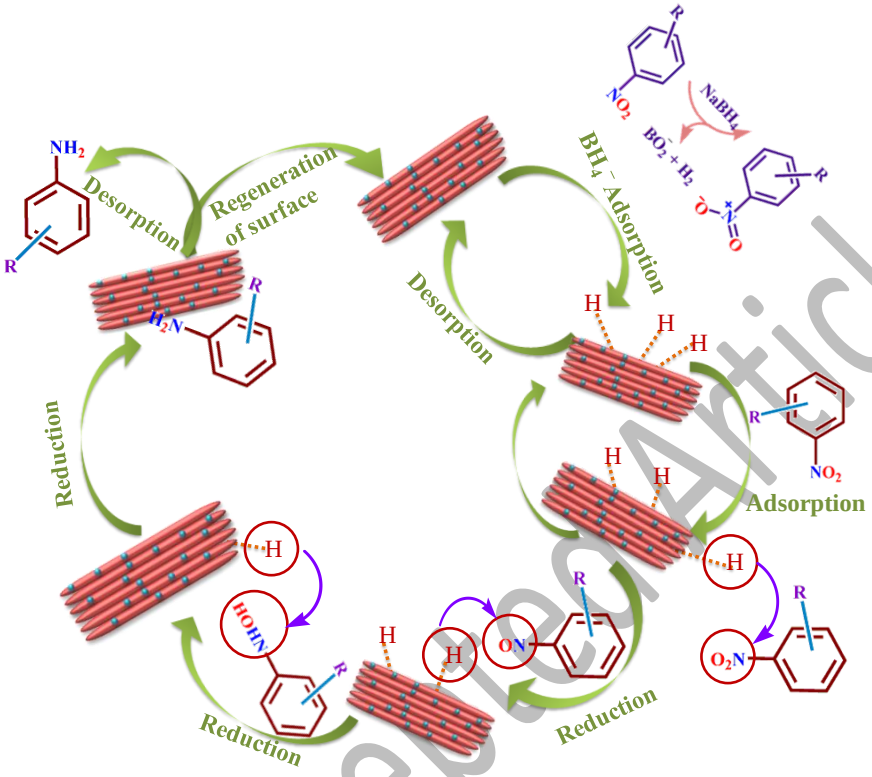

Scheme 1 The catalytic reduction mechanism of 4-NP.

The performance of the CeO_2/Bi_2WO_6 10% nanocomposite was evaluated using the Langmuir-Hinshelwood model for kinetic analysis. With a sufficiently high concentration of $NaBH_4$ solution relative to 4-NP concentration, the investigation focused on pseudo-first-order kinetics to determine the reaction rate constants (k). The kinetics were modelled using the equation $\ln(C_t/C_0) = -kt$, where C_0 and C_t represent the initial and time 't' concentrations of 4-nitrophenol, respectively [33, 34]. Fig. 5e depicts a strong linear correlation between $\ln(C_t/C_0)$ and time during the reduction process catalyzed CeO_2/Bi_2WO_6 10% nanocomposites, confirming the pseudo-first-order kinetics. The rate constant (k) was determined from the slope of this line, yielding a value of approximately 0.46 min^{-1} for the CeO_2/Bi_2WO_6 10% nanocatalyst, indicating exceptional efficiency in converting 4-NP to 4-AP. The synthesized CeO_2/Bi_2WO_6 10% nanocomposite exhibited remarkable efficacy in reducing 4-nitroaniline (4-NA) with sodium borohydride, as illustrated in Fig. 5d. Typically, the peak intensity of 4-nitroaniline decreased upon addition of CeO_2/Bi_2WO_6 10% nanocatalyst, with reduction reactions completing within 4 minutes and a corresponding rate constant (k) of 0.38 min^{-1}. Evaluation of CeO_2/Bi_2WO_6 10% nanocatalyst's stability and reusability involved collection, filtration, washing, drying, and reuse for subsequent cycles. Notably, the catalytic efficiency remained unchanged after five cycles, as confirmed by FT-IR and XRD analyses of the nanocomposite structure after each cycle. These results validate the stability and superior catalytic performance of the CeO_2/Bi_2WO_6 10% nanocomposite compared to the fresh catalyst. Consequently, the CeO_2/Bi_2WO_6 10%

IJCE-Accepted Article

nanocomposite emerges as a promising, efficient, stable, and reusable catalyst. The results of this study on reducing 4-nitrophenol using the 4-NP-$NaBH_4$-H_2O system have been compared with findings from other studies, as shown in Table 1 [32-34, 36, 52-55]. Our study compared various parameters with those reported in the literature for reducing 4-nitrophenol to 4-aminophenol (Table 1). Among the catalysts studied, the CeO_2/Bi_2WO_6 10% nanocomposite exhibited exceptional catalytic activity in reducing 4-nitrophenol (Table 1). The concentration of $NaBH_4$ and the amount of nanocatalyst were found to influence the reduction time of 4-nitrophenol significantly. Interestingly, the concentrations used in all entries were higher than those in our study, which impacted the reduction time. Moreover, our study found that the rate constant was higher than previously reported values. The dosage of the catalyst in our study was lower compared to those given in Table 1 in. Additionally, the concentration of 4-nitrophenol in this study was higher than in previous reports. The nanocatalyst used in our study was fabricated without expensive or toxic materials, making it suitable for practical applications.

Table 1 Comparison of catalytic activity of diverse reported catalysts for reducing 4-NP by $NaBH_4$.

Entry	Catalyst	$NaBH_4$ conc.	Catalytic activity (%)	Catalyst amount	Time (min)	Ref.
1	ACMNPs	10 mM	100%	10 mg	18	[52]
2	NiO/AlMCM-41	20 mM	100%	4 mg	6	[32]
3	Mag-MMO	50 mM	100%	3 mg	1	[53]
4	NiO NPs	20 mM	100%	4 mg	21	[33]
5	$Au/Pt/SnO_2$	200 mM	100%	6 mg	8	[54]
6	Cu-AG-sponge	200 mM	100%	20 mg	11	[55]
7	Ni-AG-sponge	200 mM	100%	20 mg	16	[55]
8	$CuCo_2O_4/BiVO_4$	50 mM	100%	1 mg	18	[36]
9	$CoFe_2O_4$/ZrMCM4125%	20 mM	100%	5mg	6	[34]
10	CeO_2/Bi_2WO_6 10%	20 mM	100%	1 mg	10	This work

Catalytic reduction of Cr(VI) ions by CeO_2/Bi_2WO_6 10% nanocomposite

Chromium (VI) poses a significant threat to various biological organisms, making its removal from water imperative. Researchers have dedicated efforts to mitigate the toxic effects of Cr(VI), with a crucial treatment method involving its reduction to Cr(III) [41-45, 56]. However, Cr(III) exhibits relative inertness and lower solubility in water. Catalysts play a vital role in this process, facilitating the electron transfer to the metal's high valence state, acting as an electron acceptor. The catalytic potential of the CeO_2/Bi_2WO_6 10% nanocomposite was explored, and UV-Vis spectroscopy monitored its activity. UV-Vis spectra depicted distinct absorption peaks for Cr(VI) ions in aqueous solution, with a characteristic λ_{max} of 372 nm (Fig. 6).

RSC Accepted Article

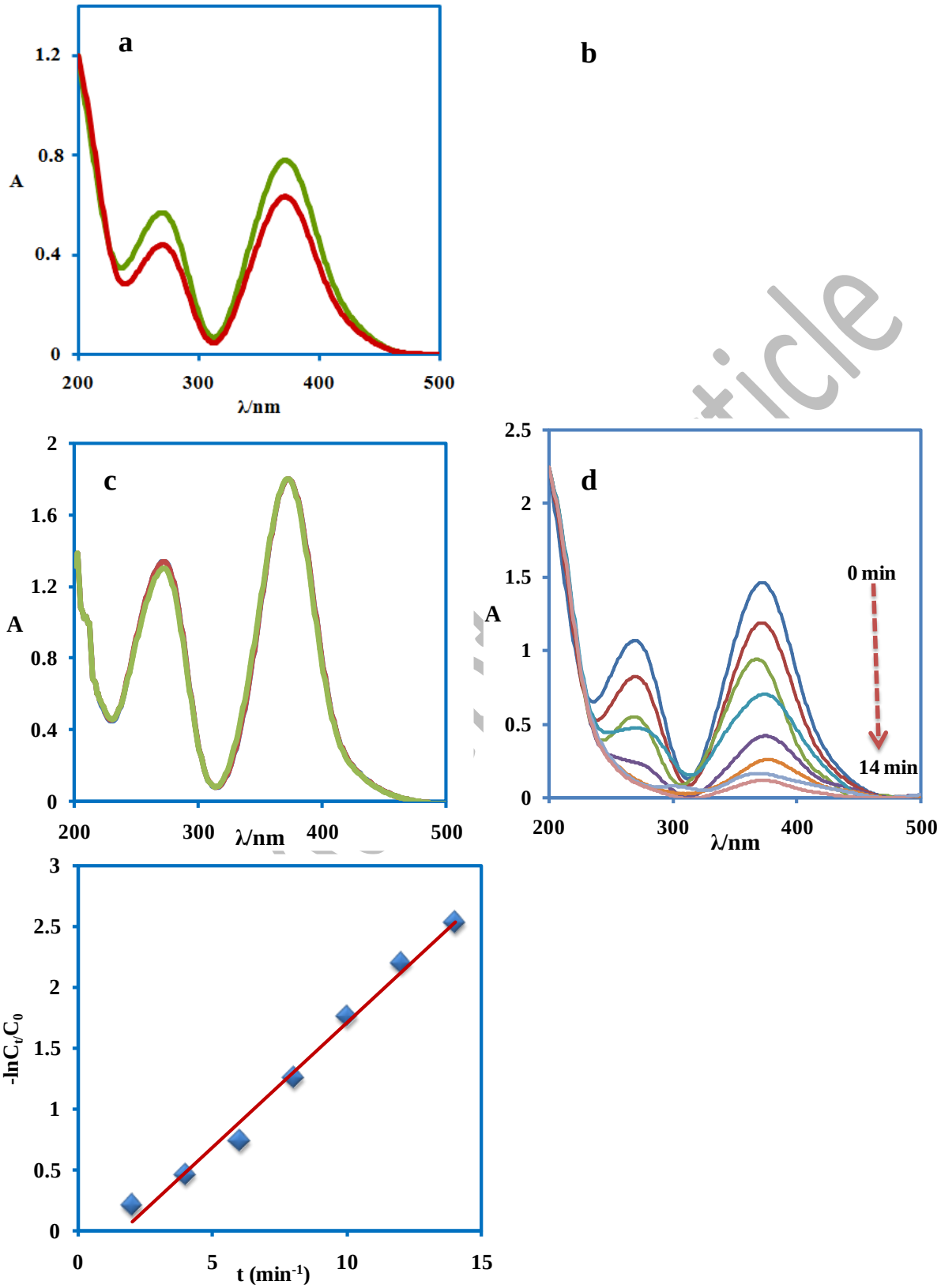

Fig. 6 Reduction of Cr(VI) with (a) just CeO_2/Bi_2WO_6 10% nanocomposite, (b) just $NaBH_4$, (c) both CeO_2/Bi_2WO_6 10% nanocomposite and $NaBH_4$, (d) plot of $-ln(C_t/C_0)$ against time.

The absorption peak at 372 nm steadily diminished with rising reaction time, accompanied by vanishing yellow color, confirming the successful reduction of Cr(VI) within 14 minutes using CeO_2/Bi_2WO_6 10% as the catalyst (Fig. 6) [34]. To assess the catalytic nature, a blank experiment without the nanocatalyst showed a slight change in peak intensity for Cr(VI) after 60 minutes (Fig. 6a). Similarly, an experiment with only CeO_2/Bi_2WO_6 10% nanocatalyst revealed no catalytic reduction of Cr(VI) after more than 60 minutes (Fig. 6b). The reduction of Cr(VI) adhered to pseudo-first-order kinetics, given the excess of $NaBH_4$ compared to Cr(VI). The constant rate (K) was calculated as 0.205 min^{-1}, as shown in Fig. 6c. The CeO_2/Bi_2WO_6 10% nanocatalyst demonstrated sustained high catalytic activity and structural stability during the reduction reaction.

Reduction of organic dye pollutants

The research investigated the degradation of carcinogenic cationic dyes, particularly methylene blue (MB) and rhodamine B (RhB), utilizing $NaBH_4$ as an environmentally friendly reductant and CeO_2/Bi_2WO_6 10% as a catalyst. The results of MB and RhB reduction reaction are illustrated in Fig. 7a and b. Throughout the experimental timeline, noticeable reductions in the peaks associated with MB and RhB were evident. MB displayed absorption peaks at 662 and 616 nm and the degradation of MB was accomplished within 4 minutes, achieving a 100% degradation rate. Similarly, the degradation of RhB reached completion in a mere 10 minutes, also attaining a 100% degradation rate. The absence of a nanocatalyst impeded the progress of the reaction, underscoring the pivotal role of CeO_2/Bi_2WO_6 10% as an effective nanocatalyst in facilitating dye degradation. The calculated rate constants for MB and RhB, were found to be 1.3 min^{-1} and 0.43 min^{-1}, respectively (Fig.7c). The Langmuir-Hinshelwood mechanism [52] provides a detailed understanding of the dye degradation process. According to this mechanism, both the dye and BH_4^- ions undergo adsorption onto the surface of the CeO_2/Bi_2WO_6 10% catalyst. As a surface mediator, the catalyst enables the transfer of electrons from BH_4^- ions to the dyes. This intermediary function of CeO_2/Bi_2WO_6 10% effectively lowers the energy barrier between the reactant and the product, facilitating the completion of the degradation reaction and evolution of H_2 gas. Compared with other reported methods this study shows excellent activity toward degradation of dyes and reaching higher TOC removal at shorter times [57-59].

IJCCE-Accepted Article

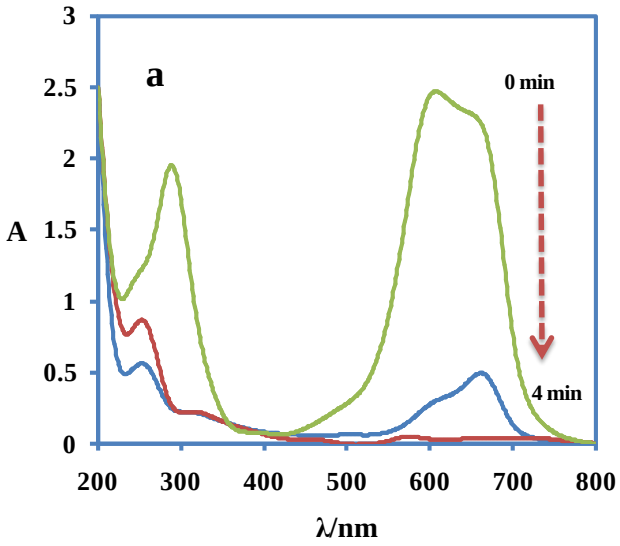

b

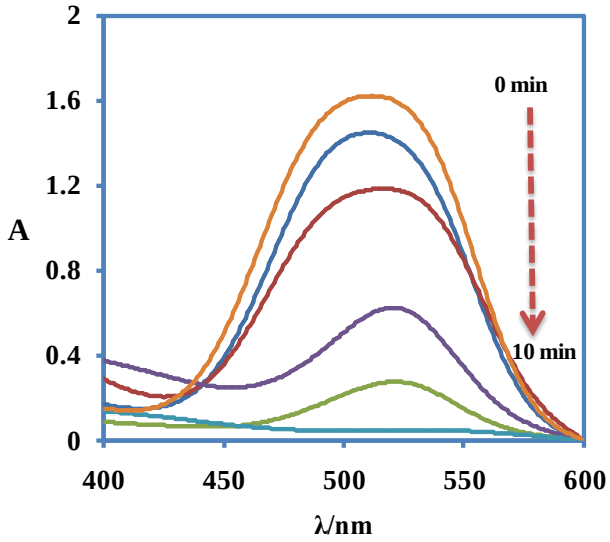

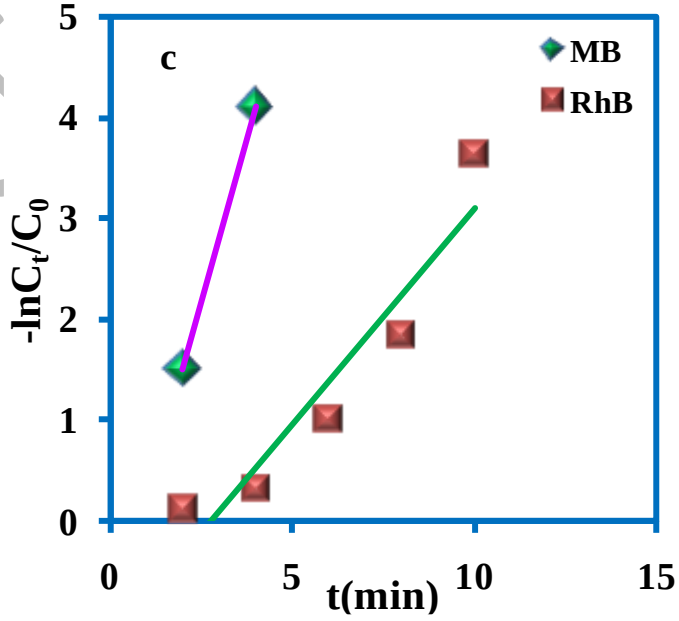

IJCRT Accepted Article

Fig.8 Reduction of (a) MB, (b) RhB with $NaBH_4$ and CeO_2/Bi_2WO_6 10% nanocomposite, (c) plot showing pseudo-first order law ($-\ln (C_t/C_o)$) versus reaction time.

CONCLUSIONS

In this study, Bi_2WO_6, CeO_2 and CeO_2/Bi_2WO_6 nanocomposites (5 %, 10 %, and 20% by weight) were successfully constructed. The efficacy of nanocomposites is contingent upon factors such as temperature, pH values of the solutions, and the molar ratio of starting materials. These variables collectively play a pivotal role in shaping the nanocomposite's structure. The nanocomposites exhibit exceptional performance as heterogeneous nanocatalysts for reducing toxic nitroaromatic compounds (4-NP and 4-NA), Cr(VI) ions, and dye pollutants (RhB, MB). Moreover, they are cost-effective, readily obtainable, and easily recoverable and possess the potential to replace expensive materials commonly employed in environmental remediation in wastewater. Their structural flexibility allows for modifications, optimizing their properties for practical applications.

CONFLICT OF INTEREST

There is no conflict of interest to declare.

IJCCE-Accepted Article

References

[1] Siriwong P., Thongtem T., Phuruangrat A., Thongtem S., Hydrothermal synthesis, characterization, and optical properties of wolframite $ZnWO_4$ nanorods, *CrystEngComm* **13**: 1564-1569 (2011).

[2] Siriwong P., Thongtem T., Phuruangrat A., Thongtem S., Hydrothermal synthesis, characterization, and optical properties of wolframite $ZnWO_4$ nanorods, *CrystEngComm* **13**: 1564-1569 (2011).

[3] Nam D., Lee G., Kim J., Interface engineering of CeO_2 nanoparticle/ Bi_2WO_6 nanosheet nanohybrids with oxygen vacancies for oxygen evolution reactions under alkaline conditions, *RSC Adv*., **13**: 8873 (2023)

[4] Gokula Krishnan S.A., Abinaya S., Arthanareeswaran G., Govindaraju S., Yun K., Surface-constructing of visible-light Bi_2WO_6/CeO_2 nanophotocatalyst grafted PVDF membrane for degradation of tetracycline and humic acid, *J. hazard. Mater.*, **421**: 126747 (2022).

[5] Issarapanacheewin S., Wetchakun K., Phanichphant S., Kangwansupamonkon W., Wetchakun N., A novel CeO_2/Bi_2WO_6 composite with highly enhanced photocatalytic activity, *Materials Letters*. **156**:28-31 (2015).

[6] Issarapanacheewin S., Wetchakun K., Phanichphant S., Kangwansupamonkon W., Wetchakun N., Photodegradation of organic dyes by CeO_2/Bi_2WO_6 nanocomposite and its physicochemical properties investigation, *Ceramics International*. **42**:16007-16 (2016).

[7] Bhoi Y.P., Rout D.P., Mishra B., Photocatalytic Chemoselective Aerobic Oxidation of Thiols to Disulfides Catalyzed by Combustion Synthesized Bismuth Tungstate Nanoparticles in Aqueous Media *J. Clust. Sci*. **27**: 267–284 (2016).

[8] Wang D., Xue G., Zhen Y., Fu F., Li D., Monodispersed Ag nanoparticles loaded on the surface of spherical Bi_2WO_6 nanoarchitectures with enhanced photocatalytic activities, *J. Mater. Chem*. **22**: 4751–4758 (2012).

[9] Wang D., Zhen Y., Xue G., Fu F., Liu X., Li D., Synthesis of mesoporous Bi_2WO_6 architectures and their gas sensitivity to ethanol, *J. Mater. Chem*. **C1**: 4153–4162 (2013).

[10] Liu Y.J., Cai R., Fang T., Wu J.G., Wei A., Low temperature synthesis of Bi_2WO_6 and its photocatalytic activities, *Mater. Res. Bull*. **66**: 96–100 (2015).

[11] Alfaro S.O., Cruz A.M., Synthesis, characterization and visible-light photocatalytic properties of Bi_2WO_6 and $Bi_2W_2O_9$ obtained by co-precipitation method, *Appl. Catal. A Gen*. **383**: 128–133 (2010).

[12] Zhang G.K., Lu F., Li M., Yang J.L., Zhang X.Y., Huang B.B., Synthesis of nanometer Bi2WO6 synthesized by sol–gel method and its visible-light photocatalytic activity for degradation of 4BS, *J. Phys. Chem. Solids*, **71**: 579–582 (2010).

[13] Zhang F.J., Xie F.Z., Liu J., Zhao W., Zhang K., Rapid sonochemical synthesis of irregular nanolaminar-like Bi_2WO_6 as efficient visible-light-active photocatalysts, *Ultrason. Sonochem*. **20**: 209–215 (2013).

[14] Mi Y., Zeng S., Li L., Zhang Q., Wang S., Liu C., Sun D., Solvent directed fabrication of Bi_2WO_6 nanostructures with different morphologies: Synthesis and their shape-dependent photocatalytic properties, *Mater. Res. Bull*. **47**: 2623–2630 (2012).

[15] Abd El-Monaem E. M., Abd El-Latif M. M., Eltaweil, A. S., El-Subruiti G. M., Cobalt Nanoparticles Supported on Reduced Amine-Functionalized Graphene Oxide for Catalytic Reduction of Nitroanilines and Organic Dyes, *Nano***, 16**: 2150039 (2021).

[16] Sallam S. A., El‑Subruiti G. M., Eltaweil A. S., Facile Synthesis of Ag–γ-Fe_2O_3 Superior Nanocomposite for Catalytic Reduction of Nitroaromatic Compounds and Catalytic Degradation of Methyl Orange, *Catalysis Letters*, **148**: 3701–3714 (2018).

IJCE-Accepted Article

[17] Ma Y., Wu X., Zhang G., Core-shell Ag@ Pt nanoparticles supported on sepiolite nanofibers for the catalytic reduction of nitrophenols in water: Enhanced catalytic performance and DFT study, *Appl. Catal. B Environ.*, **205**: 262–270 (2017).

[18] Panigrahi S., Basu S., Praharaj S., Pande S., Jana S., Pal A., Ghosh S. K., Pal T., Synthesis and Size-Selective Catalysis by Supported Gold Nanoparticles: Study on Heterogeneous and Homogeneous Catalytic Process, *J. Phys. Chem. C*, **111**: 4596-4605 (2007).

[19] Kim M., Bae S., Immobilization and characterization of Fe(0) catalyst on NaOH-treated coal fly ash for catalytic reduction of p-nitrophenol, *Chemosphere*, **212**: 1020–1029 (2018).

[20] Bae S., Gim S., Kim H., Hanna K., Effect of $NaBH_4$ on properties of nanoscale zero-valent iron and its catalytic activity for reduction of p-nitrophenol, *Appl. Catal. B Environ*., **182**: 541–549 (2016).

[21] Ai L., Li L., Efficient removal of organic dyes from aqueous solution with ecofriendly biomass-derived carbon@montmorillonite nanocomposites by one-step hydrothermal process, *Chem. Eng. J.*, **223**: 688–695 (2013).

[22] Zhang H., Jiang M., Zhang D., Xia Q., Decomposition of 4-nitrophenol by ozonation in a hollow fiber membrane reactor, *Chem. Eng. Commun*., **197**(3): 377–386 (2009).

[23] Jiang P., Zhou J., Zhang A., Zhong Y., Electrochemical degradation of p-nitrophenol with different processes, *J. Environ. Sci.*, **22**(4): 500–506 (2010).

[24] Kumar Dutta R., Verma S., Enhanced ROS generation by ZnO-ammonia modified graphene oxide nanocomposites for photocatalytic degradation of trypan blue dye and 4-nitrophenol, *J. Environ. Chem. Eng.*, **5**(5): 4776–4787 (2017).

[25] Liu Z.: Yang C., Qiao C., Biodegradation of p-nitrophenol and 4-chlorophenol by Stenotrophomonas sp, *FEMS Microbiol. Lett.*, **277**(2): 150–156 (2007) .

[26] Modirshahla N., Behnajady M., Mohammadi-Aghdam S., Investigation of the effect of different electrodes and their connections on the removal efficiency of 4-nitrophenol from aqueous solution by electrocoagulation, *J. Hazard. Mater*., **154**:(1–3), 778–786 (2008).

[27] Elfiad A., Galli F., Boukhobza L.M., Djadoun A., Boffito D.C., Low-cost synthesis of Cu/α-Fe_2O_3 from natural $HFeO_2$: application in 4-nitrophenol reduction, *J. Environ. Chem. Eng.*, **8**(5): 104214 (2020).

[28] Ghosh B.K., Ghosh N.N., Applications of metal nanoparticles as catalysts in cleaning dyes containing industrial effluents: a review, *J. Nanosci. Nanotechnol.*, **18**(6): 3735–3758 (2018).

[29] Wang C., Zhang H., Feng Gao., Shang C. S., Wang N. Z., Multifunctional Pd@MOF core–shell nanocomposite as highly active catalyst for p-nitrophenol reduction, *Catal. Commun.*, **72**: 29–32 (2015).

[30] Tokazhanov G., Ramazanova E., Hamid S., Bae S., Lee W., Advances in the catalytic reduction of nitrate by metallic catalysts for high efficiency and N_2 selectivity: a review, *Chem. Eng. J.*, **384**: 123252 (2020).

[31] Wunder S., Polzer F., Lu Y., Mei Y., Ballauff, M. Kinetic analysis of catalytic reduction of 4-nitrophenol by metallic nanoparticles immobilized in spherical polyelectrolyte brushes, *J. Phys. Chem. C*, **114**: 8814–8820 (2010).

[32] Derikvand Z., Rahmati F., Azadbakht A., Nano NiO/AlMCM-41, a green synergistic, highly efficient and recyclable catalyst for the reduction of nitrophenols, *Appl. Organomet. Chem.*, **33**: e4864 (2019).

[33] Derikvand Z., Azadbakht A., Amiri Rudbari H., Synthesis, Characterization, Crystal Structure and Supramolecular Interactions of a New Ni (II) Compound Based on l-Histidine and Dipicolinic Acid; New

UCCE-Accepted Article

Solid State Precursor for NiO Nanoparticles and Its Catalytic Activity for Nitrophenol Reduction, *J. Inorg. Organomet. Poly. Mater.*, **29**(2): 502-516 (2019).

[34] Bahrami, M., Derikvand Z., Fabrication of a new magnetic $CoFe_2O_4$/ZrMCM-41 nanocomposite: Simple construction and application for fast reduction of Cr(IV) and nitroaromatic compounds, *J. Mol. Struct.*, **1254**: 132367 (2022).

[35] Kassem A.A., Abdelhamid H.N., Fouad D.M., Ibrahim S.A., Catalytic reduction of 4- nitrophenol using copper terephthalate frameworks and CuO@C composite, *J. Environ. Chem. Eng.*, **9**: 104401 (2021).

[36] Mirzaee Valadi F., Gholami M. R., Synthesis of $CuCo_2O_4$/$BiVO_4$ composites as promise and efficient catalysts for 4-nitrophenol reduction in water: Experimental and theoretical study, *J. Environ. Chem. Eng.*, **9**: 105408 (2021).

[37] Min K.I., Choi, Chung J.S., Ahn Y.M., Ryoo, W.S., Lim R., p-Aminophenol synthesis in an organic/aqueous system using Pt supported on mesoporous carbons, *Appl. Catal. A Gen.*, **337**: 97-104 (2008).

[38] Ishida T., Haruta M., Towards Sustainable Chemistry, *Angew. Chem. Int. Ed.*, **46**: 7154-7156 (2007).

[39] Phuruangrat A., Wannapop S., Sakhon T., Kuntalue B., Thongtem T., Thongtem S., Characterization and photocatalytic properties of $BiVO_4$ synthesized by combustion method, *J. Mol. Struct*. **1274**: 134420 (2023).

[40] Yayapao O., Thongtem T., Phuruangrat A., Thongtem S., Synthesis and characterization of highly efficient Gd doped ZnO photocatalyst irradiated with ultraviolet and visibl eradiations, *Mater. Sci. Semicond. Process.* **39**: 786–792 (2015).

[41] Litter M.I., Last advances on TiO_2-photocatalytic removal of chromium, uranium and arsenic, *Curr. Opin. Green Sustainable Chem.*, **6**: 150–158 (2017).

[42] Meichtry J. M., Slodowicz M., Cancelada L., Destaillatsc H., Litter M., Sonochemical reduction of Cr(VI) in air in the presence of organic additives: What are the involved mechanistic pathways? *Ultrason. Sonochem*., **48**: 110–117 (2018).

[43] Eduardo Bortot Coelho F., Candelario V. M., Magno Rodrigues Araújo E., Lúcia Santos Miranda T., Magnacca G., Photocatalytic Reduction of Cr(VI) in the Presence of Humic Acid Using Immobilized Ce-ZrO_2 under Visible Light. *Nanomaterials*, **10**: 779 (2020).

[44] Omer A.M., Abd El-Monaem E.M., Eltaweil A. S., Novel reusable amine-functionalized cellulose acetate beads impregnated aminated graphene oxide for adsorptive removal of hexavalent chromium ions, *Int. J. Biol. Macromol*., **208**: 925–934 (2022).

[45] Omer A. M., Abd El-Monaem E. M., Abd El-Latif M. M., El-Subruiti G. M., Eltaweil A. S., Facile Fabrication of Novel Magnetic ZIF-67 MOF@Aminated Chitosan Composite Beads for the Adsorptive Removal of Cr(VI) from Aqueous Solutions, *Carbohyd. Polym.*, **265**: 118084 (2021).

[46] Zhong S., Zhang F., Yu B., Zhao P., Jia L., Zhang S., Synthesis of PVP-Bi_2W_{O6} photocatalyst and degradation of tetracycline hydrochloride under visible light, *J. Mater. Sci. Mater. Electron*., **27**: 3011 (2016).

[47] Qamar M., Elsayed R.B., Alhooshani K. R., Ahmed M. I. Bahnemann D. W., Highly Efficient and Selective Oxidation of Aromatic Alcohols Photocatalyzed by Nanoporous Hierarchical Pt/Bi_2WO_6 in Organic Solvent-Free Environment, *ACS Appl. Mate. Interfaces*, **7**: 1257-1269 (2015).

[48] Chen Y., Zhang Y., Liu C., Lu A., Zhang W., Photodegradation of Malachite Green by Nanostructured Bi_2WO_6 Visible Light-Induced Photocatalyst, *Int. J. Photoenergy*, 510158 (2012).

Accepted Article

[49] Rahimi R., Pordel S., Rabbani M., Synthesis of Bi_2WO_6 nanoplates using oleic acid as a green capping agent and its application for thiols oxidation, *J. Nanostruct. Chem*., **6**:191–196 (2016).

[50] McDevitt N.T., Baun W.L., Infrared absorption study of metal oxides in the low frequency region (700-240 cm^{-1}), *Spectrochim. Acta*, **20**: 799-808 (1964).

[51] Ankita, Chahal S., Singh S., Kumar L., Gupta., V., Kumarf S., Kumar S., Kumar P., Gd doped Cerium Oxide for organic dye degradation and tuning of magnetic properties, *Mat. Sci. Engin.B*, **300**; 117049 (2024).

[52] Saxena M., Saxena R., Fast and efficient single step synthesis of modified magnetic nanocatalyst for catalytic reduction of 4-nitrophenol, *Mate. Chem. Phys*.**, 276**: 125437 (2022).

[53] Meira A. C. R., Tremarin B. G., Cursino A. C. T., de Oliveira Basso R. L., Bail A., Giona R. M., In-situ preparation of a bismuth-based magnetic composite for catalytic reduction of 4-nitrophenol, *Mate. Chem. Phys.*, **277**: 125519 (2022).

[54] Jana S., Konar S., Chandra Mitra B., Mondal A., Mukhopadhyay S., Fabrication of a new heterostructure Au/Pt/SnO_2: An excellent catalyst for fast reduction of para-nitrophenol and visible light assisted photodegradation of dyes, *Mater. Research Bulletin*, **141**: 111351 (2021).

[55] Kamal, T.; Asiri, A. M.; Ali, N. Catalytic reduction of 4-nitrophenol and methylene blue pollutants in water by copper and nickel nanoparticles decorated polymer sponges, *Spectrochim. Acta A* **2021**, 261, 120019.

[56] Moghimian S., Azarmi F., Sangpour P., Heydari M., Mohammadian Fard Z., Tajabadi F., Rtimi S., Bagher M., Enhanced photocatalytic reduction of Cr (VI) using Ag@AgCl/RGO/CuO nanocomposite under visible light, *J. Photochem. and Photobio. A* **452**: 115584 (2024).

[57] Ankita, Chahal S., Singh S., Kumar L., Gupta V., Kumar S., Kumar S., Kumar P., Gd doped Cerium Oxide for organic dye degradation and tuning of magnetic properties, *Mate. Sci. Eng*. **B300**: 117049 (2024).

[58] Arul V., Sethuraman M.G., Facile green synthesis of fluorescent N-doped carbon dots from Actinidia deliciosa and their catalytic activity and cytotoxicity applications, *Opt. Mater*. **78**: 181–190 (2018).

[59] Shariatzadeh S. M. R., Salimi M., Fathinejad H., Hassani Joshaghani A., Synthesis, Characterization, and Photocatalytic Application of α-Fe_2O_3/α-$AgVO_3$ Nanocomposite for Removal of Methylene Blue from Aqueous Media, *Iran. J. Chem. Chem. Eng*. **42**: 1192-1205 (2023).

IJCCE Accepted